

High Performance Supercapacitor based on Polypyrrole /Melamine Formaldehyde Resin Derived Carbon Material

Lifang Song¹, Yongjin Zou^{2,3,4,*}, Haitao Zhang^{2,3,4}, Cuili Xiang^{2,3,4}, Hailiang Chu^{2,3,4}, Shujun Qiu^{2,3,4}, Erhu Yan^{2,3,4}, Fen Xu^{2,3,4}, Lixian Sun^{2,3,4}

¹School of Materials Science and Engineering, Chang'an University, Xi'an 710061, P.R. China

²Guangxi Key Laboratory of Information Materials, Guilin University of Electronic Technology, Guilin 541004, P.R. China

³Guangxi Collaborative Innovation Center of Structure and Property for New Energy Materials, Guilin 541004, P.R. China

⁴Guangxi Talent Center of Fundamental and Application for Advanced Functional Materials, Guilin 541004, P.R. China

*E-mail: zouy@guet.edu.cn, sunlx@guet.edu.cn

Received: 7 November 2016 / Accepted: 12 December 2016 / Published: 30 December 2016

In this study, N-doped super-activated carbon material was synthesized using melamine formaldehyde (MF) resin as carbon source and sequent KOH-activation method. Polypyrrole nanofibers (PPy) were further polymerized on the MF resin derived carbon (MFC). The PPy/MFC composite possesses high surface area, which is suitable for high performance supercapacitor electrode materials. Electrochemical measurements indicate the hybrid PPy/MFC electrode yielded the highest specific capacitance of 336.8 F g⁻¹ at a current density of 1 A g⁻¹ (in 6 M KOH). The PPy/MFC electrode also keeps a high capacitance retention ratio of 94.3% after 3000 cycles. Given the potential massive production and excellent electrochemical performance, The PPy/MFC nanocomposites are promising electrode materials for supercapacitor applications.

Keywords: Supercapacitor; N-doped super-activated carbon; Melamine formaldehyde resin; Polypyrrole, Nanocomposite

1. INTRODUCTION

Supercapacitors have recently attracted much attention due to their good reversibility, fast recharge ability, and long cycling stability [1-3]. Currently, supercapacitors have been commonly used in portable devices, energy management, and memory back-up systems [4]. Nevertheless, the drawbacks of supercapacitors, such as poor energy density, low specific capacitance, and self-discharging, have still been considered as main problems for the widespread use of supercapacitors [5].

There are many factors affecting the performance of the supercapacitors, including electrode materials, electrolyte, current collector, structure et al. Among these factors, the electrode material is one of the most important issues that should be concerned [5]. The favorable supercapacitor electrode materials should have high electrical conductivity, large surface area, good chemical stability and low cost. Such a strong demand enables porous carbon to be a promising supercapacitor electrode material, which can satisfy the parameters mentioned previously [6]. However, the weakness of the carbon-based materials is lack of active component, which leads to poor volumetric capacities. Therefore, developing new nanoporous carbon-based materials with improved capacitance as well as a simple synthesis method is still a challenge [5].

To boost the capacitance of carbon-based materials, Doing the carbon materials with heteroatoms (such as nitrogen or oxygen) has been embraced as an effective approach [6,7]. Particularly, the nitrogen functionalized carbon-based materials not only can improve the specific capacitance, but improve the conductivity and wettability to electrolyte solution of carbon materials. Therefore, much attention has been paid to the preparation of nitrogen-doped carbon electrode materials [8-10]. For instance, Li and coworkers prepared monodispersed N-doped hollow mesoporous carbon nanospheres by using resorcinol-formaldehyde resin as a carbon precursor and melamine as a nitrogen source [5]. Zhang et al. investigated the synthesis N-doped carbon aerogels by carbonizing the commercial melamine sponge. The resulting materials exhibited unique properties for supercapacitor and oxygen reduction electrocatalyst [11].

On the other hand, conducting polymers have attracted much attention for supercapacitors owing to their redox property, high electronic conductivity, facile synthesis procedure, and good stability [12-15]. Among the conducting polymers, polypyrrole (PPy) is one of the promising candidates for supercapacitors. However, PPy suffers from low cyclic stability and poor conductivity, which hinders its application in commercial supercapacitors [16]. Increasing the cyclic stability and conductivity of PPy in electrochemical capacitors is still a challenge in energy material for electrochemical capacitors. An integration of PPy and carbon nanomaterials (such as graphene and carbon nanotubes) allows improved electrochemical performance [17]. However, the preparation of graphene or CNTs are time consuming and difficult for synthesis in a large scale.

Therefore, in this study, melamine formaldehyde resin derived carbon (MFC) and PPy are combined to fabricate supercapacitor materials. The PPy/MFC composite displayed a fine synergistic effect between the PPy and MFC. Electrochemical measurements demonstrate that PPy/MFC electrode has a high specific capacitance of 336.8 F g^{-1} at a current density of 1 A g^{-1} , good rate capability and cycling stability in 6 M KOH electrolyte.

2. MATERIALS AND METHODS

2.1. Preparation of MFC

All the chemicals were analytical grade and used as purchased, except for pyrrole, which was distilled before use. Melamine, formaldehyde, ammonium persulfate and pyrrole were obtained from Sigma-Aldrich (USA). Deionized water was used in all the processes. The MF resin was prepared according an established procedure as described in reference [18]. Briefly, melamine (3.0 g) and

formaldehyde (13 mL) were dissolved in 14 mL deionized water with stirring at room temperature. The pH was adjusted to 8.5 with 0.1 M NaOH solution. The mixture was heated to 65 °C under a static condition until the solution became transparent MF resin. Next, the MF resin was dried at 100 °C for 4 h under vacuum. Calcination was carried out in a quartz tubular furnace at 800 °C for 5 h under N₂ flow, and then cooled to room temperature [18]. The as-prepared sample was denoted as MFC. MFC was chemically activated by heating a MFC-KOH mixture (KOH/MFC at a weight ratio of 2:1) to 600 °C for 1 h under a N₂ atmosphere. The solids were collected and washed with deionized water to neutral pH. Finally, the MFC sample was dried in a vacuum oven at 80 °C for 24 h.

2.2. Preparation of PPy/MFC binary nanocomposites

Pyrrrole was polymerized on the surface of MFC in an aqueous solution using ammonium persulfate as the oxidant. Briefly, MFC (0.1 g) was dispersed in 100 mL of deionized water and ultrasonicated for 2 h. Then, 0.1 M of pyrrole was added to the MFC suspension with stirring for 1 h. Subsequently, ammonium persulfate solution (2 g in 20 mL of deionized water) was added slowly to the MFC suspension. After stirring for 4 h, the product was collected by filtering and then washed thoroughly with deionized water and methanol. For comparison, PPy was also prepared in the same way.

2.3. Preparation of the electrodes

The nanocomposite used for the electrode was fabricated by mixing 80 wt% of the prepared samples with 10 wt% carbon black and 10 wt% polyvinylidene fluoride binder to form a uniform slurry. Next, 100 µL of ethanol was added to the mixtures in an agate mortar. The slurries were pressed onto nickel foam current collectors under a pressure of 20 MPa.

2.4. Instruments and analysis

Chemical structure of the samples was studied using Fourier-transform infrared (FTIR) (Nicolet 6700 spectrometer, USA). Scanning electron microscopy images were obtained on a JSM-6360LV microscope (JEOL Ltd., Japan) and TEM (transmission electron microscopy) analysis was conducted on a JEOL JEM-2000EX electron microscope operated at 20 kV. X-ray diffraction (XRD) was performed with a Philips 1820 diffractometer. N₂ adsorption/desorption isotherms were performed with an AUTOSORB-2 surface area analyzer (Autosorb iQ2, Quantachrome Instruments, USA) at 77 K. Cyclic voltammetry (CV), electrochemical impedance spectroscopy (EIS), and galvanostatic charge and discharge (GCD) measurements were conducted using a potentiostat (Zahner-Elektrik, Kronach, Germany) equipped with a three-electrode in a 6 M KOH solution. The working electrode is the as-prepared electrode. A platinum foil electrode and a saturated calomel electrode were used as the counter and reference electrodes, respectively. All the experiments were performed at room temperature. GCD tests were carried out in a potential range between -1.0 and 0 V. The specific

capacitances were calculated from the CVs and discharging curves according to the equations in elsewhere [3].

3. RESULTS AND DISCUSSION

3.1 Physical and Chemical Characterization of PPy/MFC

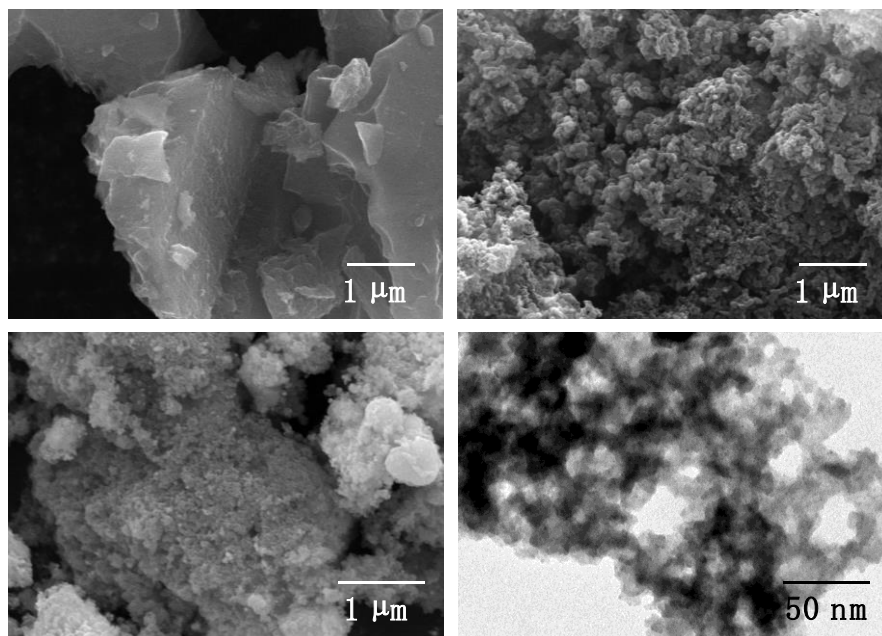


Figure 1. SEM images of (a) MFC, (b) PPy and (c) PPy/MFC. TEM images of (d) PPy/MFC.

The as-prepared samples were imaged with SEM and TEM (Figure 1). The SEM image of MFC sample in Figure 1a composed of irregular granules with typical edge and corner features. The pure PPy consisted of spherical agglomerates with a diameter of ~ 90 nm (Figure 1b). In the SEM images of the composite, PPy nanoparticles are well attached on the MFC substrate, which covered almost the whole MFC particle surface (Figure 1c). The TEM image (Figure 1d) further approves that PPy nanoparticles are decorated on the surface of MFC.

Figure 2 shows the XRD patterns of the composite. The MFC yielded a peak at $2\theta=26.4$ [11], corresponding to 002 graphite crystallites diffraction peak. This peak is also observed in the XRD pattern of PPy/MFC, indicating that the MFC were incorporated in the composite. The spectrum of the pure PPy includes a broad peak in the region of $2\theta = 20\text{--}30^\circ$, indicating that the PPy conducting polymer was amorphous [19].

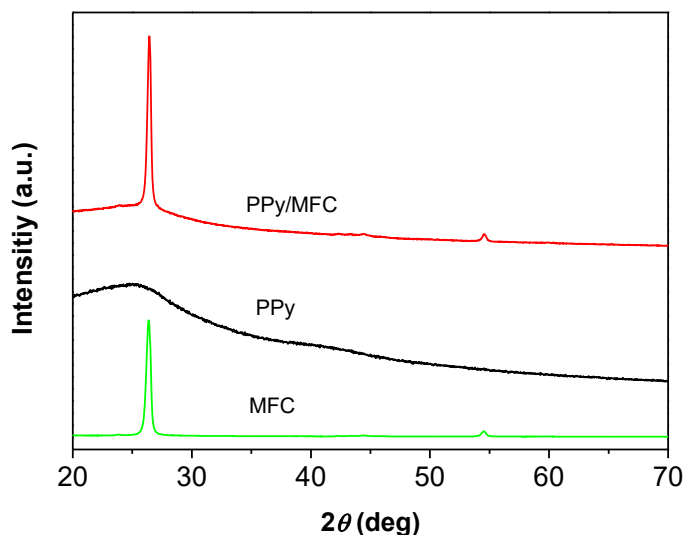


Figure 2. XRD patterns of the MFC, PPy, and PPy/MFC composite.

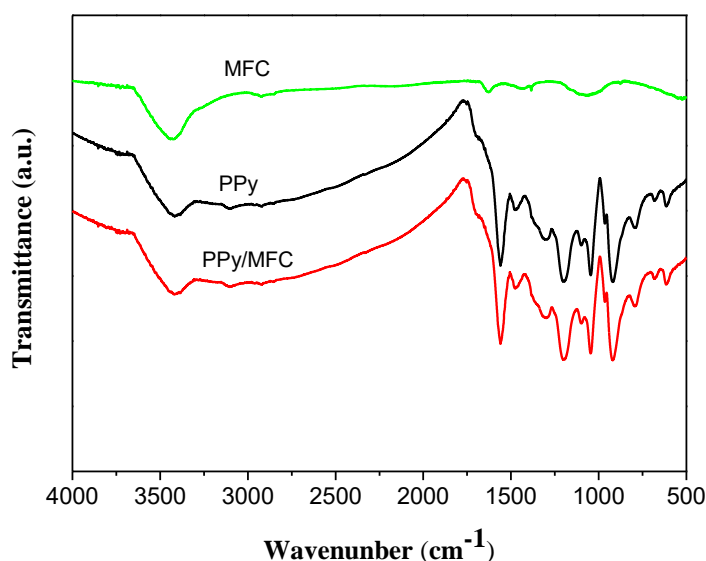


Figure 3. FTIR spectra of MFC, PPy, and PPy/MFC.

The FTIR spectra of MFC, PPy, and PPy/MFC are shown in Figure 3. The broad absorption bands at 3443 and 1637 cm^{-1} in MFC are assigned to the O–H stretching vibration which may be due to vibrations of hydroxyl groups and adsorbed water and the characteristic vibration of C–N bond, respectively. In the spectra of PPy, peaks at 1562 , 1469 and 3410 cm^{-1} corresponds to C–C, C–N and N–H stretching vibration in the pyrrole ring, respectively [20]. The peak around 1100 cm^{-1} depicts the C=N stretching vibration in the PPy. In addition, peaks at 2855 and 2962 cm^{-1} are assigned to the symmetric and asymmetric vibration of CH_2 [20]. These bands can also be found in the PPy/MFC spectrum, which confirmed presence of PPy in the nanocomposites.

The surface area the obtained materials were examined by means of nitrogen sorption technique. Figure 4 shows the N_2 adsorption/desorption isotherms of the prepared samples. The BET surface areas for the PPy, MFC, and PPy/MFC samples are 96.5 , 1028.7 , 274.1 $\text{m}^2 \text{g}^{-1}$, respectively. MFC shows largest surface area. Furthermore, MFC exhibits a type IV isotherm with a sharp capillary

condensation step, indicating the presence of mesopores [21]. Meanwhile, in the PPy/MFC composite, the deposition of PPy on MFC decreases the surface area, which could be attributed to the blocking the pores of the MFC.

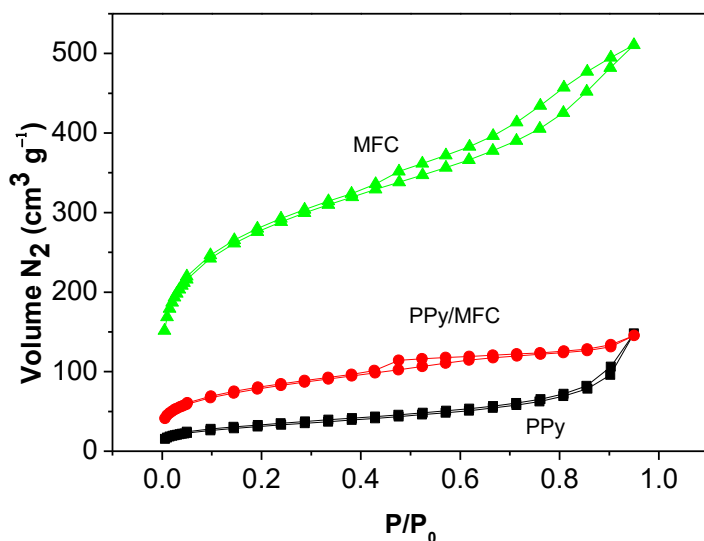


Figure 4. N₂ adsorption/desorption isotherms of the MFC, PPy, and PPy/MFC composite.

3.2 Electrochemical performance

CV was enlisted to evaluate the electrochemical performance of MFC, PPy, and PPy/MFC electrodes in 6 M KOH solution.

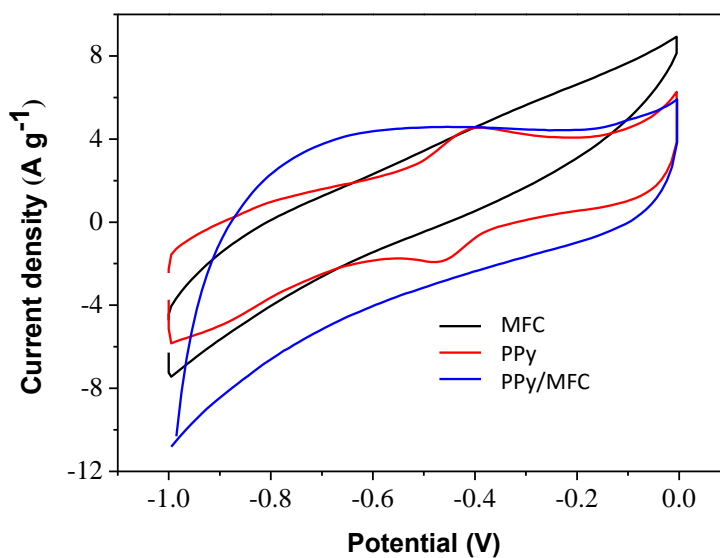


Figure 5. The CV curves of the PPy/MFC, MFC, and PPy at scan rate of 10 mV s⁻¹ in 6 M KOH electrolyte.

Figure 5 shows the CV curves of the three electrodes obtained at the same scan rate of 10 mV s^{-1} . CV curve of MFC and PPy/MFC show a deformed rectangular shape, indicating the coexistence of an electric double-layer capacitance and pseudocapacitance, which is attributed to the redox reaction of pseudocapacitive N atoms [21]. PPy/MFC possesses the best specific capacitance 340.5 F g^{-1} at a 10 mV s^{-1} sweep rate, followed by 213.2 , 171.6 F g^{-1} for PPy, MFC, respectively. These results clearly revealed the improved effect of N-doping and a conducting polymer improvement. The porous structure of MFC increases the accessible surface area of the electrochemically active N atoms for charge transfer [21]; the PPy with unique properties can also enhance the charge storage, rendering PPy/MFC the highest capacitance.

Figure 6a show the detained CV behaviors of PPy/MFC at different scan rates from 10 to 200 mV s^{-1} . The CV curves demonstrated quasi-rectangular shape, indicating the combination of electric double-layer capacitance and redox reactions in the PPy/MFC electrode, which relate to the heteroatom functionalities of the material.

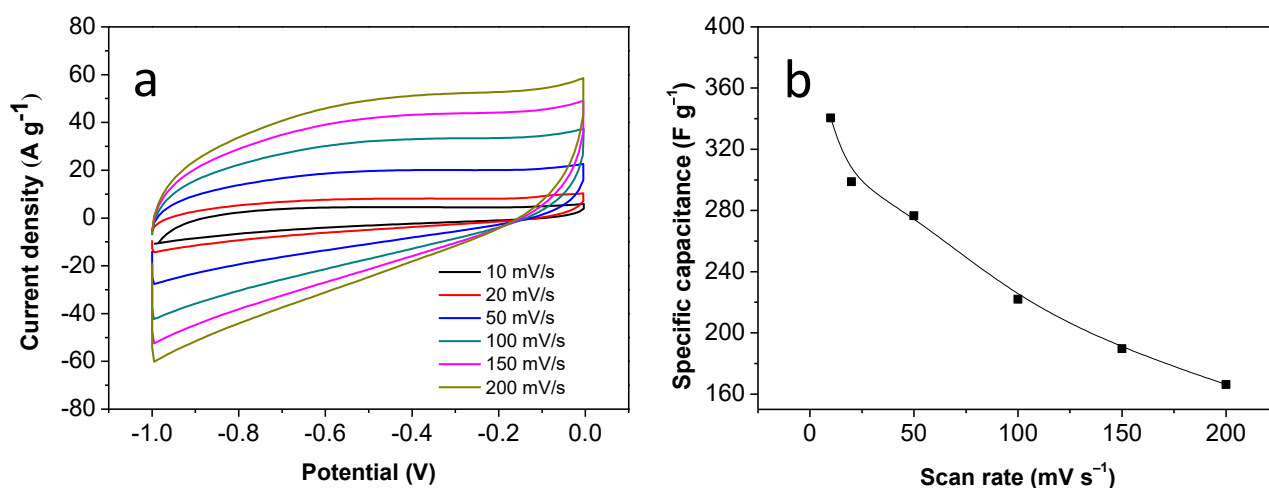


Figure 6. (a) CV curves of the PPy/MFC electrode at various scan rates in 6 M KOH electrolyte; (b) Specific capacitance of PPy/MFC calculated from CV curves versus scan rates.

The specific capacitances of PPy/MFC were calculated and plotted with the scan rates in Figure 6b. The specific capacitance of PPy/MFC is 340.5 F g^{-1} at the scan rate of 5 mV s^{-1} , which is considerably larger than most carbon-based materials and metal oxides materials [2,17]. The specific capacitance still retains $>150 \text{ F g}^{-1}$ under a high current rate of 200 mV s^{-1} , indicating its good high-rate capability.

EIS can provide the electronic/ionic conductivity information during the charging/discharging progress [17]. The semicircular part of EIS at higher frequencies corresponds to the electron transfer-limited process, which controls the electron transfer kinetics of the redox reaction at the electrode interface. While the straight line at the low frequency region is attributed to the diffusion process correspond to a diffusive resistance. Figure 7 shows the resulting Nyquist plots of the EIS spectra for the PPy, MFC, and PPy/MFC composite electrodes. The charge transfer resistance values for the PPy/MFC, MFC, and PPy electrodes were 0.5 , 38 and $42 \text{ } \Omega$, respectively. The charge-transfer

resistance value of PPy/MFC is very small, indicating a negligible interfacial electron-transfer resistance.

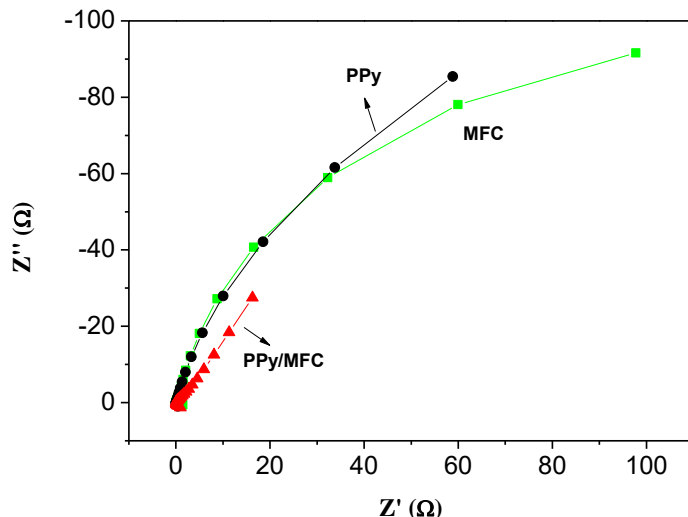


Figure 7. Nyquist plots of the EIS for PPy, MFC, and PPy/MFC electrodes.

The GCD measurements were carried out at a current density of 1 A g^{-1} and shown in Figure 8. All curves are almost triangle shape with some deviation. The observed deviation in linearity is mainly due to doping of N atom in the MFC and the presence of pseudocapacitive PPy [22]. The specific capacitance values were calculated to be 171.2, 224.9, and 336.8 F g^{-1} for the MFC, PPy, and PPy/MFC electrodes, respectively. These results are in good agreement with the data obtained from CV curves. We further compared obtained results with references presented in recent years (summarized in Table 1). Obviously, PPy/MFC exhibits much a higher specific capacitance value than those of reported systems. The overall excellent performance is attributed to the combined effect of N-doped porous carbon as well as unique properties of PPy.

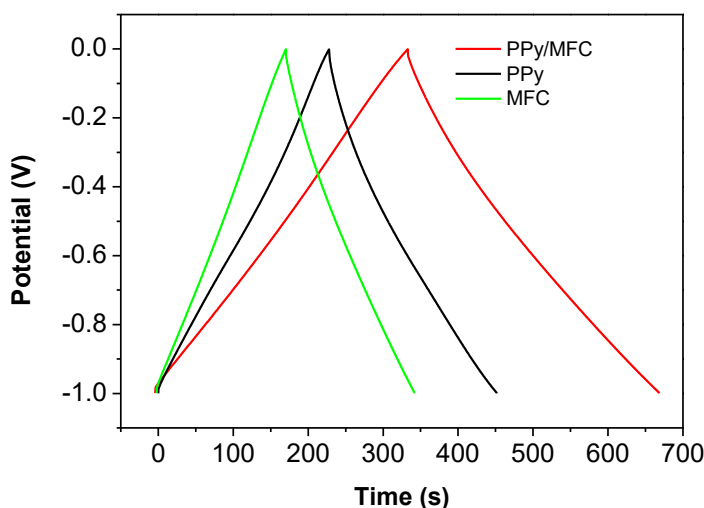


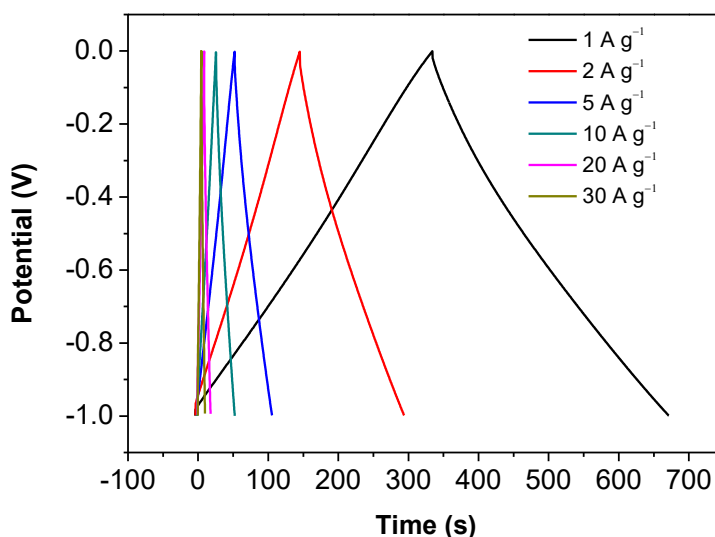
Figure 8. Charge/discharge curves of the PPy/MFC, MFC, and PPy at 1 A g^{-1} in 6 M KOH electrolyte.

Table 1. Comparison of the specific capacitance value of the PPy/MFC electrode with literatures

Sample	Capacitance measured at ($A g^{-1}$)	Specific capacitance ($F g^{-1}$)	Electrolyte	Reference
CNTs/PPy/CNTs/MF	0.4	184	KCl	[17]
RGO-MF	0.3	76.8	NaCl	[23]
N-doped GC	1	293	KOH	[24]
Carbon-G-A	1	202.7	KOH	[25]
N-doped ACS	0.5	312	KOH	[26]
N-HCSs	0.5	266.9	KOH	[27]
α -MnMoO ₄	1.6	200	NaOH	[28]
N-RCs	0.5	250	Na ₂ SO ₄	[29]
PPy/MFC	1	336.8	KOH	This work

The GCD curves at current densities of 1, 2, 5, 10, 20, and 30 $A g^{-1}$ are shown in Figure 9. The specific capacitance was calculated to be 336.8, 297.6, 286.3, 265.3, 184.2 and 156.1 $F g^{-1}$ at discharge a current density of 1, 2, 5, 10, 20, and 30 $A g^{-1}$, respectively. As expected, the specific capacitance decreased when the current density increased. Even a current density as high as 30 $A g^{-1}$, the PPy/MFC electrode still retained 46.3% of its specific capacitance at a current of 1 $A g^{-1}$.

Cycling stability is one of the critical factors for the performance of supercapacitors. In this study, the long-term cycling stability of PPy/MFC electrode was examined at current density of 1 $A g^{-1}$. As seen from Figure 10, specific capacitance of PPy/MFC electrode kept almost constant with slight fluctuations. PPy/MFC electrode retained relatively high capacitance value of 317.5 $F g^{-1}$ after 3000 cycles, about 94.3% of the initial cycle, indicating an excellent electrochemical stability.

**Figure 9.** Charge/discharge curves of PPy/MFC electrode at different densities of 1, 2, 5, 10, 20 and 30 $A g^{-1}$.

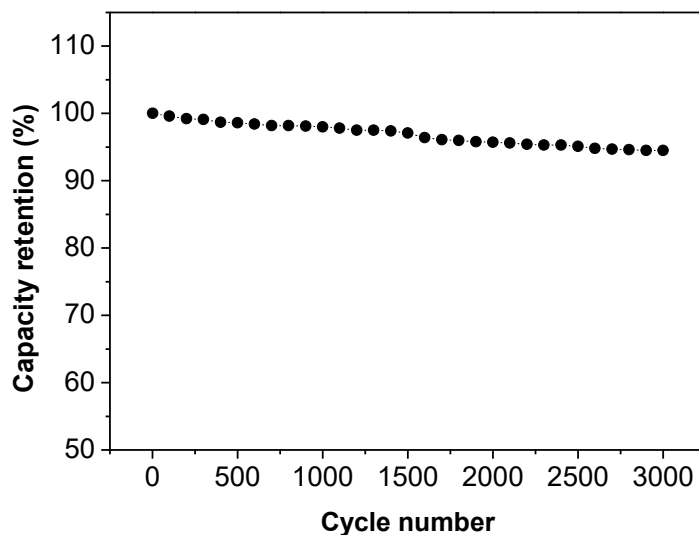


Figure 10. Cycling test of the PPy/MFC electrode at a current density of 1 A g^{-1} .

4. CONCLUSIONS

In conclusion, PPy/MFC nanocomposite was prepared using MF resin as carbon source and sequent polymerization of PPy on MFC. The PPy/MFC nanocomposite was used as supercapacitor electrode materials. Galvanostatic charge/discharge experiments show that PPy/MFC has a very high specific capacitance (336.8 F g^{-1} at 1 A g^{-1}). It also demonstrates excellent cyclic stability, with 94.3% capacitance retention for up to 3000 cycles. Therefore, we believe that the PPy/MFC nanocomposite is promising candidate for supercapacitor applications to meet the demand for high power applications.

ACKNOWLEDGEMENTS

Financial supports from the NSFC (51502021, U1501242, 51561006, 51261005, 51461010, 51401059, 51361005, 51371060, and 51461011), National Science Foundation for Post-doctoral Scientists of China (Grant No.2015M570805), Fundamental Research Funds for the Central Universities (Grant No.310831161011) the Guangxi Natural Science Foundation (2016GXNSFFA380012 and 2015GXNSFAA139282), Opening Fund of Guangxi Key Laboratory of Information Materials (151001-K), and the Innovation Project of Guangxi Graduate Education (2016YJXC23) are acknowledged.

References

1. Z. Q. Wen, M. Li, S. J. Zhu, T. Wang, Q. Guo, L. Liu. *Int. J. Electrochem. Sci.*, 11 (2016) 23–33.
2. Y. Yang, F. Yang, S. Lee, X. Li, H. Zhao, Y. Wang, S. Hao, X. Zhang. *Electrochim. Acta*, 191 (2016) 1018–1025.
3. Y. Zou, Q. Wang, C. Xiang, Z. She, H. Chu, S. Qiu, F. Xu, S. Liu, C. Tang, L. Sun. *Electrochim. Acta*, 188 (2016) 126–134
4. M. Kota, X. Yu, S.H. Yeon, H.W. Cheong, H.S. Park. *J. Power Sources*, 303 (2016) 372–378.
5. C. Liu, J. Wang, J. Li, M. Zeng, R. Luo, J. Shen, X. Sun, W. Han, L. Wang. *ACS Appl. Mater. Interfaces*, 8(2016)7194–7204.

6. W. Yan, L. Wang, C. Chen, D. Zhang, A.J. Li, Z. Yao, L.Y. Shi, *Electrochim. Acta*, 188 (2016) 230–239.
7. Z. Wang, L. Sun, F. Xu, X. Peng, Y. Zou, H. Chu, L. Ouyang, M. Zhu. *RSC Adv.*, 6(2016)1422–1427.
8. G. Sun, L. Ma, J. Ran, B. Li, X. Shen, H. Tong. *Electrochim. Acta*, 194 (2016) 168–178.
9. K. Gopalakrishnan, A. Govindaraj, C. Rao. *J. Mater. Chem. A*, 1(2013)7563–7565.
10. B. Cao, B. Zhang, X. Jiang, Y. Zhang, C. Pan. *J. Power Sources*, 196(2011)7868–7873.
11. J. Zhang, G. Chen, Q. Zhang, F. Kang, B. You. *ACS Appl. Mater. Interfaces*, 7(2015)12760–12766.
12. X. Liu, N. Wen, X. Wang, Y. Zheng, *ACS Sustainable Chem. Eng.*, 3(2015)475–482.
13. K.V. Sankar, R.K. Selvan. *J. Power Sources*, 275 (2015) 399–407.
14. J. Zhou, T. Zhu, W. Xing, Z. Li, H. Shen, S. Zhuo, *Electrochim. Acta*, 160 (2015) 152–159.
15. W. Lin, K. Xu, J. Peng, Y. Xing, S. Gao, Y. Ren, M. Chen. *J. Mater. Chem. A*, 3(2015) 8438–8449.
16. H. Mahdavi, P. K. Kahriz, H. G. Ranjbar, T. Shahalizade. *J Mater Sci: Mater Electron.*, 27 (2016) 7407–7414.
17. F. Liu, G. Han, Y. Chang, D. Fu, Y. Li, M. Li. *J. Appl. Polym. Sci.* 2014, DOI: 10.1002/APP.39779.
18. S. Moua, Y. Lu, Y. Jiang, *Appl. Surf. Sci.*, 384 (2016) 258–262.
19. S. Sahoo, S. Dhibar, G. Hatui, P. Bhattacharya, C. K. Das, *Polymer* 54 (2013) 1033–1042.
20. C. Xiang, D. Jiang, Y. Zou, H. Chu, S. Qiu, H. Zhang, F. Xu, L. Sun, L. Zheng, *Ceram. Int.* 41(2015)6432–6438.
21. J. Zhang, G. Chen, Q. Zhang, F.Kang, B. You, *ACS Appl. Mater. Interfaces* 7(2015) 12760–12766.
22. Q. Wang, Y. Zou, C. Xiang, H. Chu, S. Liu, E. Yan, F. Xu, L. Sun, C. Tang, *Int. J. Electrochem. Sci.*, 11 (2016) 5679 – 5690.
23. X. Gu, Y. Yang, Y. Hu, M. Hu, J. Huang, C. Wang, *RSC Adv.*, 4(2014)63189–63199.
24. L. Sun, C. Tian, Y. Fu, Y. Yang, J. Yin, L. Wang, H. Fu, *Chem. Eur. J.* 20(2014) 564–574.
25. X. Huang, Q. Wang, X.Y. Chen, Z.J. Zhang, *J. Electroanal. Chem.*, 748 (2015) 23–33.
26. Y. Wang, H. Xuan, G. Lin, F. Wang, Z. Chen, X. Dong, *J. Power Sources*, 319 (2016) 262–270.
27. H. Sun, Y. Zhu, B. Yang, Y. Wang, Y. Wu, J. Du, *J. Mater. Chem. A*, 4(2016)12088–12097.
28. B. Senthikumar, R. K. Selvan, D. Meyrick, M. Minakshi, *Int. J. Electrochem. Sci.*, 10 (2015) 185 – 193.
29. K. Sun, D. Guo, X. Zheng, Y. Zhu, Y. Zheng, M. Ma, G. Zhao, G. Ma, *Int. J. Electrochem. Sci.*, 11 (2016) 4743–4754.

© 2017 The Authors. Published by ESG (www.electrochemsci.org). This article is an open access article distributed under the terms and conditions of the Creative Commons Attribution license (<http://creativecommons.org/licenses/by/4.0/>).